NEUROSCIENCE

10.1126/sciadv.1600797

The elementary representation of spatial and color vision in the human retina

Ramkumar Sabesan,[1]*†‡ Brian P. Schmidt,[2†] William S. Tuten,[1] Austin Roorda[1]

The retina is the most accessible element of the central nervous system for linking behavior to the activity of isolated neurons. We unraveled behavior at the elementary level of single input units—the visual sensation generated by stimulating individual long (L), middle (M), and short (S) wavelength–sensitive cones with light. Spectrally identified cones near the fovea of human observers were targeted with small spots of light, and the type, proportion, and repeatability of the elicited sensations were recorded. Two distinct populations of cones were observed: a smaller group predominantly associated with signaling chromatic sensations and a second, more numerous population linked to achromatic percepts. Red and green sensations were mainly driven by L- and M-cones, respectively, although both cone types elicited achromatic percepts. Sensations generated by cones were rarely stochastic; rather, they were consistent over many months and were dominated by one specific perceptual category. Cones lying in the midst of a pure spectrally opponent neighborhood, an arrangement purported to be most efficient in producing chromatic signals in downstream neurons, were no more likely to signal chromatic percepts. Overall, the results are consistent with the idea that the nervous system encodes high-resolution achromatic information and lower-resolution color signals in separate pathways that emerge as early as the first synapse. The lower proportion of cones eliciting color sensations may reflect a lack of evolutionary pressure for the chromatic system to be as fine-grained as the high-acuity achromatic system.

INTRODUCTION

A single photoreceptor is sensitive to both the intensity and the wavelength of light falling on it and, therefore, confounds brightness and color signals (*1*). Our visual system ultimately constructs a representation of the external world from the output of the photoreceptor mosaic in which color and achromatic contrast are divorced (*2*, *3*). How, and which, postreceptoral neural pathways recover and segregate this multiplexed information from individual receptors remains unresolved (*4*, *5*). We addressed this outstanding question by recording visual sensations upon stimulating spectrally identified cones in human subjects with light.

There are two fundamental impediments to linking visual perception to the activity of individual retinal neurons. First, the retina is situated inside the eyeball and thus can be neither visualized nor stimulated at cellular resolution due to the eye's aberrated optics. Second, even while steadily fixating, the retina moves over spatial scales far greater than the size of a single cone, impeding the repeated and reliable stimulation of the same cell. Here, we overcome these limitations using adaptive optics (*6*) and high-speed retinal tracking (*7*–*9*) to record sensations arising from individual cones in living human retina (Fig. 1A). Studies of visual perception with small spots have previously been reported, albeit without the capacity to repeatedly target distinct cones, and hence have relied on an ensemble analysis (*10*, *11*).

BRIEF METHODS

Cone-targeted stimulation

Cone-sized spots (0.45 arc min; 543-nm wavelength; 25-nm bandwidth) were targeted on a mosaic of spectrally identified long (L), medium (M), and short (S) wavelength-sensitive cones in two male, color-normal subjects—S10001R and S20076R. The subjects reported the color of each flash. The stimuli appeared for 500 ms on a dim background subjectively adjusted to appear approximately achromatic at the start of each session. A gray background was chosen to roughly equate the resting-state activities of L- and M-cones to minimize biases in downstream neurons. In the case of a large stimulus, chromatic contrast from a gray background that increases only L-cone activity produces a reddish sensation in most subjects, whereas excursions from gray that increase only M-cone activity appear bluish green (Fig. 1B) (*12*). These percepts are thought to be represented in the visual system by spectrally opponent neurons (*13*). Although this sets an expectation on the elicited perceptual categories, the extent to which these large-field predictions will generalize to single cone–mediated percepts remains unknown.

The spatiotemporal precision of our light delivery system has been previously validated with a detection experiment carried out under threshold conditions (*7*). A model of light capture in single cones accurately predicted performance on the detection task and estimated that more than 90% of light was coupled into the targeted cone. The present study used a longer-duration flash [15 frames (500 ms) versus 1 frame (120 μs)] and targeted cones at a smaller retinal eccentricity (~1.5° versus ~3°), where cones are slightly smaller (*14*). However, the delivery error does not grow worse over the duration of the flash because the eye-tracking algorithm continues to correct for eye movement throughout (*8*). Across our subjects, targeting error, defined as the spatial offset between the intended target cone and the actual stimulus location, remained less than a quarter the size of a cone at the studied eccentricity—0.21 and 0.16 arc min (~1.0 and 0.7 μm on the retina) for S10001 and S20076, respectively, on average. The smaller size of cones at 1.5° affects expected light capture but only minimally. At this location, the model estimated 82% of light was captured by the targeted cone. On average, this predicts that, of

[1]School of Optometry and Vision Science Graduate Group, University of California, Berkeley, Berkeley, CA 94720, USA. [2]Graduate Program in Neuroscience, University of Washington, Seattle, WA 98109, USA.
*Corresponding author. Email: rsabesan@uw.edu
†These authors contributed equally to this work.
‡Present address: Department of Ophthalmology, University of Washington School of Medicine, Seattle, WA 98109, USA.

the light captured by the mosaic, less than 3% was absorbed by the neighboring six cones. Therefore, the targeted cone is expected to catch 20 to 30 times more light than the surrounding cones.

RESULTS

Sensations from single cones are repeatable

S-cones, making up 4% of the targeted cones in our study, are much less sensitive to the 543-nm stimulation wavelength and therefore would be expected to have a much higher threshold in a detection task. Despite permitting subjects to repeat stimulus presentations and using high-contrast stimuli, the mean fraction of "not seen" trials was far higher in the sample of S-cones (n = 12; mean fraction not seen = 0.62; SD = 0.17) compared to L/M-cones (n = 273; mean fraction not seen = 0.11; SD = 0.13) (t_{283} = 13.3, $P < 0.001$). Because of the spatiotemporal precision of stimulation, the percepts originating from individual cones were rarely arbitrary: Stimulation of the same cone in different sessions, sometimes many months apart, produced repeatable responses (Fig. 1C). The results we report were also largely invariant to the wavelength and chromatic contrast of the flash (figs. S1 and S2). The reliability of percepts generated in this unnatural experimental paradigm demonstrates the nervous system's ability to associate the output of an individual cone with a consistent, though often nonveridical, color sensation.

Separate populations of cones contribute to chromatic or achromatic percepts

A total of 273 L- and M-cones were targeted, and similar trends were observed between subjects. Because of the close similarity, we grouped cells across both subjects in subsequent analyses. In response to flashes that were seen, our subjects reported achromatic sensations 61.8% of the time. When red was reported (22.5% of seen trials), it was more likely to be driven by L- than M-cones (t_{271} = 7.32, $P = 3 \times 10^{-12}$), whereas green (15.7%) was more likely to come from the excitation of M-cones (t_{271} = −7.45, $P = 1 \times 10^{-12}$). Thus, L-cones tended to signal both white and red, whereas M-cones tended to signal both white and green. The observation that these color percepts roughly align with the predictions of large-field cone-isolating stimuli (see above) suggests that the same opponent neuronal circuits may be implicated in both paradigms. This finding also supports the idea that the nervous system can learn the spectral identity of individual cones (*15*, *16*).

The distribution of responses elicited from the cones in both subjects' retina is plotted as a function of stimulated cone type in Fig. 2A. Table 1 reports the frequency of dominant (most numerous) color

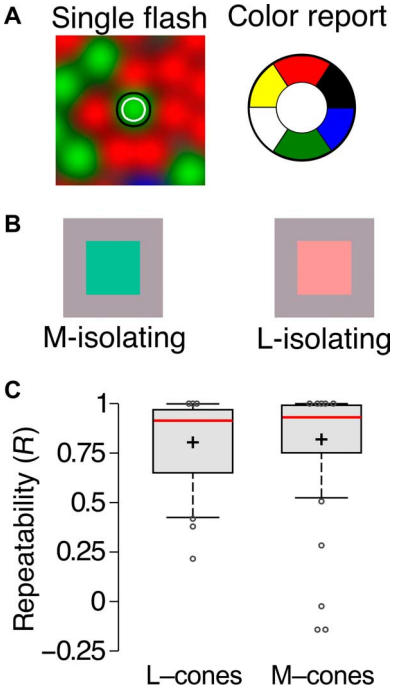

Fig. 1. Experimental design. (**A**) Schematic of the experiment. Individual cones within a classified mosaic were targeted with flashes of light (543 nm; 500 ms). Contours represent the stimuli and denote 70 and 90% capture of light over the cone. Subjects reported the color of each flash as red, green, blue, yellow, white, or not seen. (**B**) Examples of cone-isolating stimuli on an achromatic background that stimulate many cones simultaneously. M-cone–isolating conditions produce a green or greenish blue color, whereas L-cone–isolating conditions appear red. (**C**) Response repeatability across both subjects. Sixty L/M-cones were targeted in at least two sessions. The correlation coefficient (R) was computed between the responses elicited in each session. The distribution of R values across all 60 repeated cones is represented with a box-and-whisker plot. Cross, mean; red line, median; box, 25th and 75th percentiles; circles, outliers; whiskers span 9 and 91%.

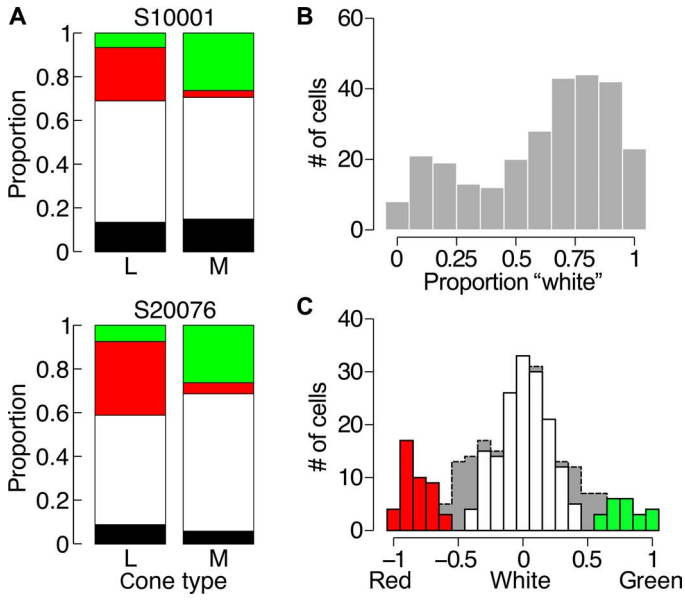

Fig. 2. Color and achromatic percepts are represented by different cell populations. (**A**) Distribution of color-naming behavior from S10001 (n = 77 and 51 for L- and M-cones, respectively) and S20076 (n = 97 and 48 for L- and M-cones, respectively). Colors correspond to the percepts reported; black indicates not seen. (**B**) Distribution of white responses elicited from all L- and M-cones (n = 273). (**C**) Distribution of RG metric across all L- and M-cones (n = 273). The red, white, and green bars represent the cones that have response purities greater than the Monte Carlo distribution mean. The gray dotted area denotes the low-purity cones (n = 48).

responses for each cone type. Note that seven L-cones most often elicited green responses, and one M-cone was dominated by red responses. Together, these cones account for 3% of the tested population, which is close to the error rate of our cone classification method (approximately 3 to 5%) (*17*).

We sought to distinguish two possible scenarios that could have generated the distribution of color and achromatic responses in our data, described above. One possibility is that all cones signal achromatic responses on a large fraction of trials but occasionally and stochastically signal a hue according to the cone-specific distributions in Fig. 2A. Alternatively, the majority of the L- and M-cones could reliably signal achromatic percepts with a small handful of cones purely signaling red or green. To distinguish these two scenarios, we first assessed the possibility that color names were assigned randomly by calculating the "response purity" of each cell (number of responses in max category/number of trials). The results of this analysis for all L- and M-cones (n = 273) revealed a high mean response purity of 0.78. A Monte Carlo resampling of all of the responses revealed that the probability of the observed distribution occurring by chance was much less than 1 in 10,000.

Table 1. Frequency of dominant color categories across L- and M-cones. Counts represent the number of L- or M-cones most frequently reporting the given color.

	White	Red	Green	Blue	Yellow
L-cones	119	48	7	0	0
M-cones	77	1	21	0	0

Next, we found that the proportion of achromatic responses across all L- and M-cones (Fig. 2B) exhibited a nonunimodal distribution (Hartigan's dip = 0.033, P = 0.035) (*18*). Most cones signaled white on a majority of trials, whereas a small group was dominated by red or green. However, this analysis does not distinguish whether the population of cells with only a few white reports (left side of Fig. 2B) was dominated by red, green, or a mix of red and green reports. To quantify the strength and distribution of color-responding cells, we defined a red-green (RG) metric (*19*) as $\frac{g-r}{T}$, where r is the number of times red was reported, g is the number of green reports, and T is the number of trials. Upon scoring the responses of each cell according to the RG metric, we found that cells were dominated by a single visual sensation: red, green, or white (Fig. 2C). The color-preferring cells in Fig. 2B were thus not a result of cones signaling both red and green percepts with high frequency. The apparent segregation of color categories into distinct populations of cells (Figs. 2 and 3 and fig. S3) is suggestive of a parallel representation of color and achromatic sensations. Moreover, these results imply that, for a large number of cones, their individual activation is not sufficient to produce a color sensation.

Spectrally opponent neighborhoods do not produce chromatic sensations

To evaluate the spatial organization of percepts arising from the cone mosaic, a response histogram for each L/M-cone from S10001 and S20076 overlaid on the spectrally classified mosaics

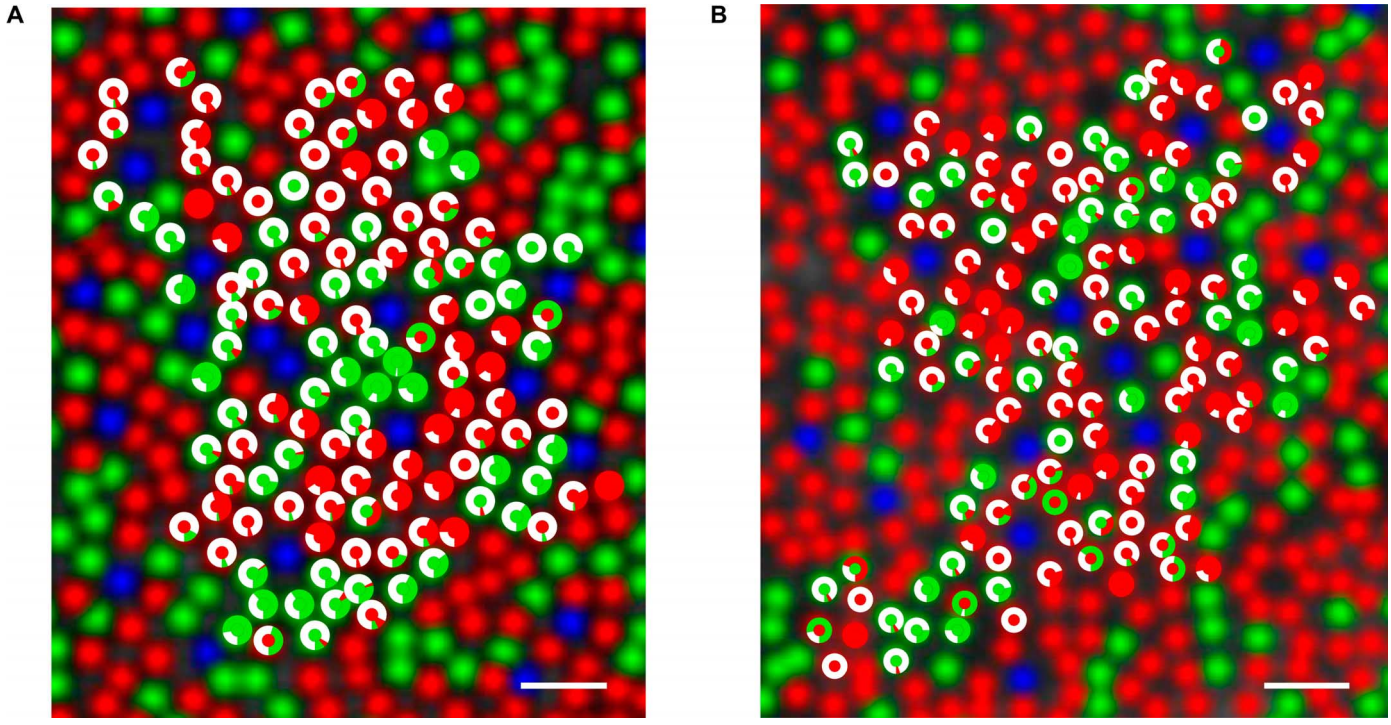

Fig. 3. Color sensations from a trichromatic cone mosaic. Color responses from individual cells are plotted over the classified cone mosaic in two subjects (blue, S-cone; green, M-cone; red, L-cone). (**A**) S10001. (**B**) S20076. The inner circles denote the cone type (same color convention as mosaics); outer circles represent a response histogram, denoting the proportion of color responses. Scale bars, 2.5 arc min.

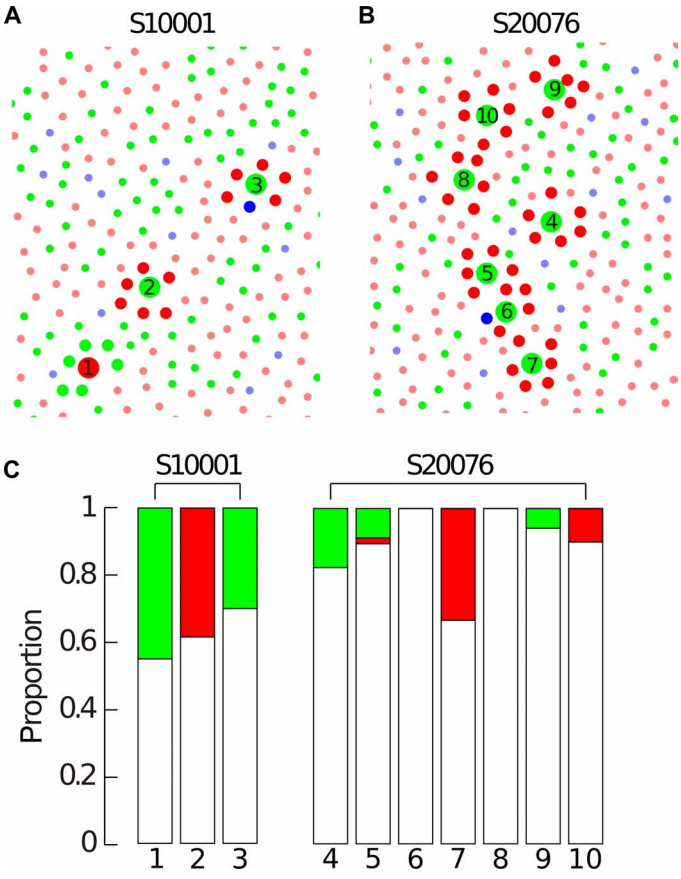

Fig. 4. Opponent neighborhoods produce achromatic sensations. Cones surrounded by neighbors of opponent type are highlighted. Large circles represent the targeted cone; medium circles highlight the six nearest neighbors. (**A**) S10001. (**B**) S20076. (**C**) Color responses from the 10 cones with pure opponent arrangements. Numbers on the *x* axis correspond to the labels on (A) and (B).

is shown in Fig. 3. As statistically confirmed by the response purity analysis, repeated stimulation of a cone tended to produce a single color report. As revealed in Fig. 2C, we did not find individual cones signaling both red and green in high proportions. A small number of cones produced occasional red or green reports together with the other color, but the frequency of this behavior was low. Because of the inherent difficulty of this task and our subjects are not perfectly reliable (Fig. 1C), we decided not to speculate on these anomalies and instead focused our analysis on the dominant response category elicited from each cone.

We found that the cones most likely to generate strong spectral opponency in a parvocellular neuron, that is, those surrounded by cones of opposing type (*20*, *21*), were not more likely to generate red or green percepts (Fig. 4 and fig. S4). Rather, all these examples, when stimulated in isolation, drove achromatic percepts on a majority of the trials.

DISCUSSION

The present study represents the first time cone photoreceptors of known spectral type have been individually targeted and activated with light in the living human retina. Despite the unusual nature of this paradigm, the subjects could use basic color terms to reliably describe their experience of these light flashes. By additionally identifying the spectral type of each targeted cone, we linked elementary color sensations to the activation of single L- or M-cones. Below, we consider the implications of these findings on our understanding of the neural circuitry mediating the appearance of color.

There is little doubt that the long-duration suprathreshold stimulation of individual cones here influences the firing of a number of different ganglion cell types. In particular, a multielectrode study demonstrated that the activation of a single cone simultaneously evoked responses in both midget (parvocellular) and parasol (magnocellular) ganglion cells (*22*). The latter has been posited to contribute to achromatic percepts (*23*, *24*). However, at the eccentricity studied here (1.5° temporal retina), midgets make up more than 90% of the ganglion cells sampling the cone mosaic (*25*). Moreover, the midget ganglion cells respond best to high-contrast, low-temporal frequency stimuli. A 500-ms suprathreshold illumination of the center cone of a midget ganglion cell receptive field, with minimal light from the spot falling on surrounding cones, represents an ideal stimulus for these cells. Therefore, our results may be particularly informative in differentiating proposals about the role of parvocellular neurons in achromatic spatial and color vision.

Near the fovea, midget ganglion cells are generally considered to have a center mechanism that receives input from only a single cone and a surround mechanism that draws indiscriminately from neighboring cones (*20*, *26*, *27*). This arrangement naturally confers L/M spectral opponency in a majority of these cells, and therefore, they are often assumed to have a central role in red-green color perception. The center-surround receptive field organization of midget ganglion cells also makes them well suited for mediating high-acuity spatial vision. Accordingly, in addition to color vision, they have also been proposed to have a role in our high-acuity achromatic spatial vision (*4*, *26*, *28*). Thus, theories about the midget system range from emphasizing their possible role in mediating color percepts to emphasizing the part they might play in mediating achromatic ones.

Depending on the theory to which one adheres about the role of midget ganglion cells in perception, our finding that stimulation of single M-cones surrounded by L-cones most often produces percepts of "white" (Fig. 4 and fig. S4) might seem surprising. As an example, consider what happens when we stimulate an M-cone with six L-cones in its immediate surround, such as those represented in Fig. 4. Light in the center excites the ON midget ganglion cell and inhibits the OFF midget with direct input from the cone. Conversely, the same M-cone excites the surround of the nearby L-OFF midgets and inhibits L-ON midget ganglion cells. Consequently, only considering the midget ganglion cells associated with a stimulated M-cone and six L-cone neighbors, our stimulus excites, to a greater or lesser extent, seven M-ON midget ganglion cells and inhibits seven L-ON ganglion cells. Therefore, if midget ganglion cells participate in color appearance, this spectrally opponent arrangement should be most efficient at eliciting chromatic percepts, but our results do not align with this expectation (Fig. 4 and fig. S4).

Over the years, since the first recordings of parvocellular neurons (*29*, *30*), two different theoretical approaches have been taken with respect to their role in vision and how chromatic and achromatic percepts might be separated. First, midget ganglion cells have been proposed to do "double duty" at the level of the retina contributing

to both high-acuity black/white vision and red-green color vision (*28*, *31*, *32*), with the two being separated at a higher level in the visual pathway. The second class of theories proposes a parallel representation in which color and luminance are separated in the retina (*33*, *34*), with parvocellular neurons responsible for a high-resolution achromatic representation of the visual scene and a sparser population signaling color in parallel. In the most recent version from this latter class of theories, the majority of parvocellular neurons are suggested to serve achromatic percepts, whereas the sparser color-coding ganglion cells have been proposed to be a small subset of midget ganglion cells (*35*, *36*).

It has been long recognized that, theoretically, chromatic and achromatic signals carried by parvocellular neurons could be separated in the cortex (*28*). Moreover, under the double-duty class hypotheses, it may be possible that the high spatial frequency nature of single-cone stimuli could favor signaling in an achromatic pathway (*23*) and thus explain the white responses reported by our subjects. However, we also discovered substantial structure to the spatial organization of color sensations at the level of the cone mosaic in both subjects. Most striking was the tendency for cells that elicit a color to cluster near each other (Fig. 3 and fig. S3). In both subjects, we found patches of two to five cones signaling green or red surrounded by larger groups of L- and M-cones predominantly signaling white. It does not seem that theories, which all midget ganglion cells do double duty, would have predicted the observed structure in the spatial organization of sensations at the level of the cone mosaic and the distinct separation of cones into populations that elicit achromatic and chromatic sensations that we observed here. In contrast, the parallel representation theories predict that color-coded ganglion cells are interspersed within a higher-density mosaic of achromatic coding cells (*33*, *34*, *36*)—exactly consistent with our observations.

In general, the visual system has adapted to the limits imposed by the spatial and spectral content of the environment. Given that the eye's optics blur the spatiochromatic structure of the natural environment, an individual cone is almost never stimulated in isolation (*27*). Thus, there may be little evolutionary pressure for the visual system to retrieve color information on the spatial scale of individual cones. The red-green system samples the visual world at a lower resolution than the achromatic system (*37*, *38*). The results from the studies reported here are consistent with the idea that the nervous system represents these two pieces of information with separate pathways that emerge as early as the photoreceptor synapse: one chiefly concerned with high-resolution achromatic vision and a second, lower-resolution color system.

MATERIALS AND METHODS

Subjects

The University of California Berkeley Institutional Review Board approved this research, and subjects signed an informed consent before participation. All experimental procedures adhered to the tenets of the Declaration of Helsinki. Two highly experienced psychophysical subjects (S10001 and S20076) with normal color vision were enrolled in the study. Mydriasis and cycloplegia were achieved with 1% tropicamide and 2.5% phenylephrine ophthalmic solutions before each experimental session. Dental impressions were used to stabilize subjects' head position.

Cone-resolved imaging and stimulation

A scanning laser ophthalmoscope equipped with adaptive optics (AOSLO) was used for imaging and stimulation of cones. Wavelengths centered at 842 and 543 nm were selected from a supercontinuum source (SuperK EXTREME, NKT Photonics) and relatively adjusted for the chromatic vergence difference of the ocular media. Both wavelengths were raster-scanned to generate a 1.2° imaging field of view on the retina. The 543-nm wavelength was chosen to minimize the difference in L- and M-cone activity. Light scattered from the retina was similarly split into separate collection assemblies for each wavelength. The 842-nm wavelength played two roles. First, a fraction (10%) of the light scattered at this wavelength was used for wavefront sensing and subsequently driving the adaptive optics correction. The rest was collected in a photomultiplier tube via a confocal pinhole and rendered into a video stream to perform real-time retinal image registration. Retinal tracking coordinates so obtained were used to drive an acousto-optic modulator, a high-speed (50 MHz) optical switch delivering 543-nm visual stimuli to the retina one pixel at a time. The spatial location of the stimuli on the retina was retrieved from the exact time stamp of when the switch was activated and differenced with the desired location to arrive at the error in stimulus delivery. Transverse chromatic aberration, the spatial offset between the imaging (842 nm) and stimulation (543 nm) wavelengths, was monitored and compensated during the experiment (*9*). Stimuli were sized ~0.45 arc min in diameter and displayed over 15 video frames (500 ms). Stimulus size was less than half the size of a cone inner segment (*14*) at the retinal eccentricity studied (~1.5°).

Recording visual sensations from individual cones

The 842-nm wavelength produced a 1.2° square that was dimly reddish purple in appearance. A background leak from the stimulus channel (543 nm) produced a slightly brighter greenish-appearing square. To extinguish these extraneous color sensations and produce a neutral viewing background, a digital light processing (DLP) projector illuminated the subject's retina in Maxwellian view (Fig. 1B). At the beginning of each session, the subject was asked to set the background to be as dim and achromatic as possible. The final chromaticity of the background (imaging raster, stimulus leak, and Maxwellian view) was measured with a color-matching technique. A second square adjacent to the background was displayed through the DLP projector. The subject then adjusted the second square until it matched in chromaticity and luminance to the adjacent background. The match was measured with a PR-650 (Photo Research) spectroradiometer. This yielded an estimate of the typical background, which had a luminance of 45 cd m^{-2} and an x, y chromaticity of 0.23, 0.30 (CIE 1931), though this varied slightly between sessions and subjects. The luminance of the stimulus (3570 cd m^{-2}) was approximately 80 times higher than the background. The power of the stimulus channel was measured with a radiometer (Newport Optical Power Meter 1830-C). Power measurements were converted into quanta. A single (3 pixel–by–3 pixel, 15-frame) flash delivered ~7.0-log quanta to the cornea.

On a subset of cones indicated in figs. S1 and S2, we altered the stimulation wavelength and intensity and undertook the same measurements. To determine the effect of slight intersession variability in background luminance and chromaticity, we measured the repeatability in visual percepts across days (figs. S2 and S4), wavelengths, and intensities.

At the beginning of each session, the experimenter marked the cones of interest on a high-resolution retinal image. Effort was made

to remain contiguous in cone selection and to repeat the experiment on a handful of cones across different days. Each cone of interest in our data set was targeted 20 times during each experimental session. Within a session, between 6 and 10 cones were tested (120 to 200 trials), with the presentation randomly interleaved among the cones to prevent subject bias. The subject was allowed to rest as needed. Responses were encoded with a handheld tablet. The subject initiated each presentation, repeating trials as needed.

A 1-s retinal video was recorded accompanying every stimulus presentation and was denoted by an audible beep. The subject then selected from six possible choices: red, green, blue, yellow, white, and not seen. Pilot trials indicated that these categories were sufficient to encompass the percepts generated under our conditions. The response was registered with another keystroke and an audible beep, different from that for video recording. A digital mark was embedded into the retinal video, corresponding to the time stamp of optical switch activation. This mark was retrieved offline using image cross-correlation and compared against the desired location to arrive at an estimate of spatial offset errors in stimulus presentation.

Associating visual percepts with cone types

Before the color sensation psychophysics reported here, the cone types (L, M, or S wavelength) comprised in the retina at 1.5° temporal eccentricity were identified using adaptive optics retinal densitometry (*17*, *39*). The cone identities in a ~0.5° patch—comprising 800 and 631 cones for S10001 and S20076, respectively—were obtained. The percentage of L-cones [L/(L + M)] in subject S10001 was 66.2% L and 66.7% L in S20076. Each cone tested psychophysically was identified with a specific spectral type by aligning the 842-nm reflectance image and the corresponding trichromatic cone mosaic map obtained from densitometry. The alignment was guided by the pattern of blood vessels in the subjects' retina, and individual cone locations remained stable across days.

Analysis

The elicited percepts were analyzed for percentage seen, color reported, neighborhood effects, and clustering of cones reporting the same percept. Except where noted, trials reported as not seen were excluded from analysis. Two hundred seventy-three L- and M-cones were used in these analyses except in select cases where low-purity cones were eliminated. The latter were defined as those cones with response purities lower than the mean of the Monte Carlo analysis (0.61). All analyses were carried out in Matlab (MathWorks).

For comparison of mean color responses across spectral classes, we treated each cone as an individual sample from a population. Therefore, we had 174 L-cone, 99 M-cone, and 12 S-cone samples. Two-tailed *t* tests were used to assess whether these sample populations differed in the mean proportion of trials that elicited a given response. S-cones were compared to L- and M-cones together to determine whether the mean number of not seen responses was higher for S-cones than for L/M-cones. Similarly, we compared whether L- and M-cone distributions differed in their mean fraction of red, green, or white responses.

As described above, we assessed the repeatability of color responses by targeting the same cone during two separate sessions (20 trials each). The degree of repeatability was then computed as the correlation coefficient (*R*) between the response distributions. For example, if the first session produced a response vector of [3, 14, 0, 0, 0] (white, red, green, blue, yellow) and the second yielded a vector of [5, 5, 5, 0, 0], the repeatability would equal 0.52. In a few cases, the same cone was targeted three times, in which case *R* was computed between all combinations of days, and the average was used as the repeatability of that cone.

The probability that the colors reported by our subjects occurred by chance was assessed with a bootstrapping procedure. First, the distribution of color responses across all L- and M-cones in the data set was computed. Color names were then randomly assigned to each of the cones by sampling from the population-wide distribution with replacement. After reassigning random color responses to each cone, the response purity of each randomized cone was determined and the mean was computed across the population. This procedure was performed 10,000 times. The distribution of mean response purities from the resampled population was then compared to the mean response purity observed in our experimental data set. The observed value (0.78) was substantially above all 10,000 resampled populations.

Clustering analysis was performed with a modified version of the density recovery profile defined by Rodieck (*40*). First, the location of each stimulated cone was identified, and the color response associated with each cone was transformed into a single number reflecting the dominant color category elicited from that cone. Cones with a purity lower than 0.61 (the mean value obtained from bootstrap analysis described above) were eliminated from this analysis. This threshold did not substantially alter the results for S10001 but did cause the analysis of red signaling cones in S20076 to lose significance. The remainder of the analysis followed the procedure described by Roorda and colleagues (*41*). Each submosaic (red or green dominated cells) was analyzed separately. For each cone in the submosaic, its nearest neighbors were computed and the distance to each like neighbor was used to generate a histogram. Histogram counts were converted to density by taking the area of each ring of distances into account. The data represented here are considered uncorrected density because edge artifacts that occur at the edge of the measured data were not taken into account. These artifacts artificially lower the density of long-range distances, because these will often include unmeasured areas of mosaic. To partially mitigate this effect, the longest distance analyzed was 5 arc min. Bootstrapping was used to assess significance. One thousand bootstrapped mosaics were created by randomly reassigning the dominant color category of each cone according to the distribution of dominant color responses observed in the data. A given ring of distances was considered statistically different from random if it exceeded 2 SDs, in either direction, from the mean of the bootstrap analysis ($P < 0.05$).

All regression analyses were carried out as described in the text using the "regstats" and "corrcoef" functions in Matlab. Two-sample *t* tests carried out on color-naming data used the "ttest2" function. Nearest neighbors were found with the "knnsearch" function. Bimodality was assessed with Hartigan's dip test (*18*), using an implementation of the algorithm downloaded from http://ringachlab.net/lab/Data.html. A *P* value was computed for the dip test using 10,000 bootstraps.

SUPPLEMENTARY MATERIALS

Supplementary material for this article is available at http://advances.sciencemag.org/cgi/content/full/2/9/e1600797/DC1

fig. S1. Wavelength invariance of color signals.

fig. S2. Intensity invariance of color signals.

fig. S3. Cones signaling color sensations are spatially clumped.

fig. S4. The influence of neighboring cones on color appearance.

REFERENCES AND NOTES

1. W. A. H. Rushton, Review lecture: Pigments and signals in colour vision. *J. Physiol.* **220**, 1–31 (1972).
2. D. H. Brainard, Color and the cone mosaic. *Annu. Rev. Vision Sci.* **1**, 519–546 (2015).
3. D. H. Foster, Color constancy. *Vision Res.* **51**, 674–700 (2011).
4. S. G. Solomon, P. Lennie, The machinery of colour vision. *Nat. Rev. Neurosci.* **8**, 276–286 (2007).
5. R. Shapley, M. J. Hawken, Color in the cortex: Single- and double-opponent cells. *Vision Res.* **51**, 701–717 (2011).
6. A. Roorda, F. Romero-Borja, W. J. Donnelly III, H. Queener, T. J. Hebert, M. C. W. Campbell, Adaptive optics scanning laser ophthalmoscopy. *Opt. Express* **10**, 405–412 (2002).
7. W. M. Harmening, W. S. Tuten, A. Roorda, L. C. Sincich, Mapping the perceptual grain of the human retina. *J. Neurosci.* **34**, 5667–5677 (2014).
8. D. W. Arathorn, Q. Yang, C. R. Vogel, Y. Zhang, P. Tiruveedhula, A. Roorda, Retinally stabilized cone-targeted stimulus delivery. *Opt. Express* **15**, 13731–13744 (2007).
9. W. M. Harmening, P. Tiruveedhula, A. Roorda, L. C. Sincich, Measurement and correction of transverse chromatic offsets for multi-wavelength retinal microscopy in the living eye. *Biomed. Opt. Express* **3**, 2066–2077 (2012).
10. H. Hofer, B. Singer, D. R. Williams, Different sensations from cones with the same photopigment. *J. Vis.* **5**, 444–454 (2005).
11. J. Krauskopf, R. Srebro, Spectral sensitivity of color mechanisms: Derivation from fluctuations of color appearance near threshold. *Science* **150**, 1477–1479 (1965).
12. M. A. Webster, E. Miyahara, G. Malkoc, V. E. Raker, Variations in normal color vision. II. Unique hues. *J. Opt. Soc. Am. A* **17**, 1545–1555 (2000).
13. R. L. De Valois, K. K. De Valois, E. Switkes, L. Mahon, Hue scaling of isoluminant and cone-specific lights. *Vision Res.* **37**, 885–897 (1997).
14. C. A. Curcio, K. R. Sloan, R. E. Kalina, A. E. Hendrickson, Human photoreceptor topography. *J. Comp. Neurol.* **292**, 497–523 (1990).
15. D. H. Brainard, D. R. Williams, H. Hofer, Trichromatic reconstruction from the interleaved cone mosaic: Bayesian model and the color appearance of small spots. *J. Vis.* **8**, 1–23 (2008).
16. N. C. Benson, J. R. Manning, D. H. Brainard, Unsupervised learning of cone spectral classes from natural images. *PLOS Comput. Biol.* **10**, e1003652 (2014).
17. R. Sabesan, H. Hofer, A. Roorda, Characterizing the human cone photoreceptor mosaic via dynamic photopigment densitometry. *PLOS One* **10**, e0144981 (2015).
18. J. A. Hartigan, P. M. Hartigan, The dip test of unimodality. *Ann. Stat.* **13**, 70–84 (1985).
19. J. Gordon, I. Abramov, H. Chan, Describing color appearance: Hue and saturation scaling. *Percept. Psychophys.* **56**, 27–41 (1994).
20. H. Kolb, D. Marshak, The midget pathways of the primate retina. *Doc. Ophthalmol.* **106**, 67–81 (2003).
21. G. D. Field, J. L. Gauthier, A. Sher, M. Greschner, T. A. Machado, L. H. Jepson, J. Shlens, D. E. Gunning, K. Mathieson, W. Dabrowski, L. Paninski, A. M. Litke, E. J. Chichilnisky, Functional connectivity in the retina at the resolution of photoreceptors. *Nature* **467**, 673–677 (2010).
22. P. H. Li, G. D. Field, M. Greschner, D. Ahn, D. E. Gunning, K. Mathieson, A. Sher, A. M. Litke, E. J. Chichilnisky, Retinal representation of the elementary visual signal. *Neuron* **81**, 130–139 (2014).
23. P. E. King-Smith, D. Carden, Luminance and opponent-color contributions to visual detection and adaptation and to temporal and spatial integration. *J. Opt. Soc. Am.* **66**, 709–717 (1976).
24. J. M. Crook, B. B. Lee, D. A. Tigwell, A. Valberg, Thresholds to chromatic spots of cells in the macaque geniculate nucleus as compared to detection sensitivity in man. *J. Physiol.* **392**, 193–211 (1987).
25. D. M. Dacey, in *Higher-Order Processing In The Visual System*, G. R. Bock, J. A. Goode, Eds. (John Wiley & Sons Ltd., 1994).
26. D. M. Dacey, O. S. Packer, Colour coding in the primate retina: Diverse cell types and cone-specific circuitry. *Curr. Opin. Neurobiol.* **13**, 421–427 (2003).
27. B. B. Lee, P. R. Martin, U. Grünert, Retinal connectivity and primate vision. *Prog. Retin. Eye Res.* **29**, 622–639 (2010).
28. C. R. Ingling Jr., E. Martinez-Uriegas, The relationship between spectral sensitivity and spatial sensitivity for the primate r-g X-channel. *Vision Res.* **23**, 1495–1500 (1983).
29. R. L. De Valois, I. Abramov, G. H. Jacobs, Analysis of response patterns of LGN cells. *J. Opt. Soc. Am.* **56**, 966–977 (1966).
30. T. N. Wiesel, D. H. Hubel, Spatial and chromatic interactions in the lateral geniculate body of the rhesus monkey. *J. Neurophysiol.* **29**, 1115–1156 (1966).
31. A. M. Derrington, J. Krauskopf, P. Lennie, Chromatic mechanisms in lateral geniculate nucleus of macaque. *J. Physiol.* **357**, 241–265 (1984).
32. R. L. De Valois, K. K. De Valois, A multi-stage color model. *Vision Res.* **33**, 1053–1065 (1993).
33. R. W. Rodieck, in *From Pigments to Perception*, A. Valberg, B. B. Lee, Eds. (Plenum Press, 1991), pp. 83–93.
34. D. J. Calkins, P. Sterling, Evidence that circuits for spatial and color vision segregate at the first retinal synapse. *Neuron* **24**, 313–321 (1999).
35. B. P. Schmidt, M. Neitz, J. Neitz, Neurobiological hypothesis of color appearance and hue perception. *J. Opt. Soc. Am. A* **31**, A195–A207 (2014).
36. B. P. Schmidt, P. Touch, M. Neitz, J. Neitz, Circuitry to explain how the relative number of L and M cones shapes color experience. *J. Vis.* **16**, 18 (2016).
37. K. T. Mullen, The contrast sensitivity of human colour vision to red-green and blue-yellow chromatic gratings. *J. Physiol.* **359**, 381–400 (1985).
38. N. Sekiguchi, D. R. Williams, D. H. Brainard, Efficiency in detection of isoluminant and isochromatic interference fringes. *J. Opt. Soc. Am. A* **10**, 2118–2133 (1993).
39. A. Roorda, D. R. Williams, The arrangement of the three cone classes in the living human eye. *Nature* **397**, 520–522 (1999).
40. R. W. Rodieck, The density recovery profile: A method for the analysis of points in the plane applicable to retinal studies. *Vis. Neurosci.* **6**, 95–111 (1991).
41. A. Roorda, A. B. Metha, P. Lennie, D. R. Williams, Packing arrangement of the three cone classes in primate retina. *Vision Res.* **41**, 1291–1306 (2001).

Acknowledgments: We thank P. Tiruveedhula, A. Boehm, H. Hofer, J. Neitz, and F. Rieke for their assistance and input in this work. **Funding:** This work was supported by the NIH Bioengineering Research Partnership (R01EY023591), National Eye Institute Cooperative Agreement (U01EY025501), NIH (R21EY021642, T32EY07031, and K23EY022412), NIH P30 EY001730, Fight for Sight postdoctoral award, American Optometric Foundation William C. Ezell Fellowship, and unrestricted grant from Research to Prevent Blindness. R.S. holds a Career Award at the Scientific Interfaces from the Burroughs Wellcome Fund. **Author contributions:** R.S., B.P.S., W.S.T., and A.R. conceived and designed the study. R.S., B.P.S., and W.S.T. established methods and collected data. R.S. and B.P.S. analyzed data and wrote the article. R.S., B.P.S., W.S.T., and A.R. reviewed and edited the article. A.R. supervised the study. **Competing interests:** A.R. has two patents on technology related to the AOSLO, which are U.S. Patent 7,118,216 (Method and apparatus for using adaptive optics in a scanning laser ophthalmoscope) and U.S. Patent 6,890,076 (Method and apparatus for using adaptive optics in a scanning laser ophthalmoscope). These patents are assigned to both the University of Rochester and the University of Houston. The patents are currently licensed to Canon Inc. (Japan). Both A.R. and the company may benefit financially from the publication of this research. **Data and materials availability:** All data needed to evaluate the conclusions in the paper are present in the paper and/or the Supplementary Materials. Additional data related to this paper may be requested from the authors.

Submitted 14 April 2016
Accepted 19 August 2016
Published 14 September 2016
10.1126/sciadv.1600797

Citation: R. Sabesan, B. P. Schmidt, W. S. Tuten, A. Roorda, The elementary representation of spatial and color vision in the human retina. *Sci. Adv.* **2**, e1600797 (2016).

The elementary representation of spatial and color vision in the human retina

Ramkumar Sabesan, Brian P. Schmidt, William S. Tuten and Austin Roorda

Sci Adv **2** (9), e1600797.
DOI: 10.1126/sciadv.1600797